Experimental Determination of Operational Pedal Cycle Frame Loads

Paul Miles, Dr. Mark Archibald
Grove City College, Grove City, PA 16127
Email: MilesPR1@gcc.edu

Abstract:

This study experimentally investigated pedalcycle frame loads and verified analytical load cases applied to vehicle design. The experimental results were compared with a Finite Element Analysis (FEA) model. The weight of the rider on the seat, road induced loads and vibrations, and the force the rider exerts on the pedals affect the stress state of the frame. Strain gages were applied to four different locations on the monotube recumbent frame. The gages were located on the top and side of the right chainstay, in front of the seat on the top of the main tube, and also on the top of the down-tube. The stress state was calculated from the raw strain data. Depending on the gage being used, the results either indicated the principal stresses or simply the axial stress. The different loading conditions tested were as follows: static, steady pedaling on smooth, mid-grade, and rough pavement, and hard acceleration on level ground and uphill. The static and hard acceleration cases were directly compared to the FEA model. The experimental results were comparable to the FEA analysis. For the cases looking at the average value, the standard deviation is also included in parentheses. For static testing, the maximum compressive principal stress was measured as -8.0 (0.1) ksi and -6.4 (.05) ksi for the chainstay and top-tube, respectively. FEA predictions at these locations were -7.4 and -6.2 ksi. The axial stress component on the down-tube was measured as -4.5(0.02) ksi, compared with -2.0 ksi predicted by FEA. The hard acceleration load case was much more complex. Peak compressive stress was measured on the chainstay, top-tube, and down-tube as -9.2, -4.7, and -4.7 ksi respectively. FEA predicted results for this load case were -8.3, -7.8, and -4.1 ksi. The complexity of the load case, coupled with unknown actual loads, explains the larger differences between FEA and experimental results. Based on experimental results, the FEA model was refined, improving the agreement between model and experiment. The stress states of a bicycle frame were successfully found experimentally, being confirmed by multiple runs under each loading condition. Based on the agreement between the two methods, the use of FEA load cases to predict stresses in pedal cycle frames was verified.

Introduction:

Stress throughout a bicycle frame varies under different loading conditions. A certain part of the frame will experience different stresses when the bike is static than it will when the bike is being pedaled. Various forces acting on the frame cause these stresses. The weight of the rider on the seat, road induced loads and vibrations, chain tension, and the force the rider exerts on the pedals, all affect the state of stress of the frame.

In order to find the state of stress, strain gauges can be applied to various locations along a frame. A strain gauge is simply an electric resistor. The gauge works on the principle that the resistance across the resistor will change as it experiences variations in length, i.e. compression of the frame corresponds to a decrease in length of the resistor, and subsequently a decrease in resistance. A single gauge can consist of several resistors, called grids, oriented in such a way as to reflect the strain in both the x- and y-directions. A rosette gauge is an example of this type of gauge. It consists of three single-axis gauges oriented as seen in Figure 1 on the right. Using this strain data, the principal stresses and the angle along which they act within the frame can be found. The principal stresses are the maximum and minimum normal stresses. To find these values the maximum shearing stress was also determined. The calculations for these quantities are seen in equations (1) and (2).

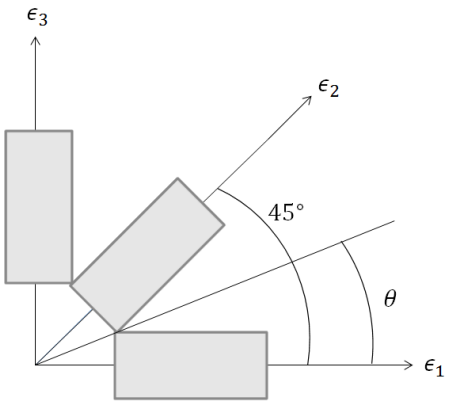

Figure 1: Rosette Strain Gauge

$$\tau_{max} = \frac{E}{\sqrt{2}(1+\mu)}[(\epsilon_1 - \epsilon_2)^2 + (\epsilon_2 - \epsilon_3)^2]^{1/2} \quad (1)$$

$$\sigma_{max}, \sigma_{min} = \frac{E(\epsilon_1+\epsilon_3)}{2(1-\mu)} \pm \tau_{max} \quad (2)$$

Where τ is the shearing stress, E is the modulus of elasticity, μ is Poisson's ratio, σ is the normal stress, and ϵ is the strain. For ϵ the subscripts (1, 2, and 3) refer to the resistor within the gauge, with 1 and 3 being perpendicular to each other and 2 being 45° from both. These equations come from the application of Mohr's circle in determining stresses. To determine the x- and y-components of the stress the principal angle was also required, which was found using equation (3).

$$\tan 2\theta = \frac{2\epsilon_2 - \epsilon_1 - \epsilon_3}{\epsilon_1 - \epsilon_3} \quad (3)$$

Due to the cyclic nature of bicycle riding, there is often a sudden change in the sign of the principal angle for areas of the frame near the pedals. It is important to note that this angle reflects the required rotation to get to the principal axis from grid 1 of the rosette gauge, i.e. the grid that produces ϵ_1 as seen in Figure 1. There are also gauges that are comprised of just a single resistor. These single-axis gauges can be used to find the axial stress by simple application of Hooke's Law as seen in equation (4).

$$\sigma = E\epsilon \quad (4)$$

For this research, both types of gauges were used and the resulting stress calculations were analyzed. The purpose of this research was to experimentally determine pedalcycle frame loads

and to create a data base of load cases to be applied to vehicle design. The results are then to be used to verify a Finite Element Analysis model.

Figure 2: Long Wheel Base Recumbent Bicycle

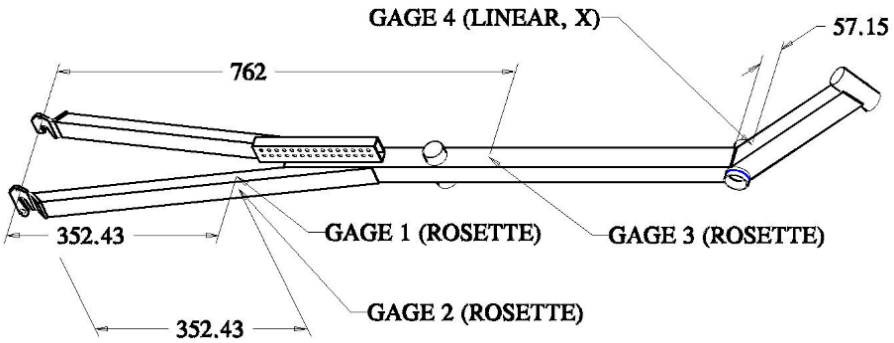

Figure 3: Frame Diagram with Gauge Positions – Dimensions are in millimeters (mm)

Equipment:

Somat E-DAQ Lite data acquisition system, Vishay Micro-Measurements general purpose strain gauges (3 rosettes and 1 linear), personal computer with SOMAT field analysis software and Matlab®

Experimental Setup:

Strain gauges were applied to four different locations on the frame to record data under different loading conditions. The gauges were located on the top and side of the right chainstay, in front of the seat on the top of the main tube, and also on the top of the down tube on the front. Three of the gauges (two on the chainstay, one on the main tube) were rosettes and the fourth

gauge was linear. The three rosette gauges were oriented on the frame such that the middle grid of the gauge ran along the long axis of the frame segment it was attached too. All data were recorded by a DAQ system mounted behind the seat of the bike. After each test case the data was transferred to a computer and converted to a text file using SOMAT Infield® a data analysis software. Matlab® code was written to determine the state of stress based on the raw strain data taken from the text file. The Matlab® code calculated the stresses and included multiple functions used to analyze the results. The code allowed the user to select the indices of the test from a plot of the raw strain data, and it also allowed the user to graphically or numerically compare the data. Depending on the gauge being used, the results either indicated the principal stresses or simply the axial stress. The different loading conditions tested were as follows: static, steady pedaling on smooth, mid-grade, and rough pavement, and hard acceleration on level ground and uphill. The static loading condition simply consisted of the rider sitting on the bike with his feet on the pedals while the bike was held in place with wheels on the ground. Steady riding meant that the rider attempted to maintain a consistent pedaling force at all times. Steady pedaling was done on three different surfaces. The hard acceleration case meant that the rider exerted maximum pedaling force for the duration of the test period. The rider simply attempted to pedal as fast as possible going on level ground and uphill. For each test case, the gauges were first calibrated to account for resistance changes due to temperature. For dynamic conditions, tests were performed by initializing a test and then flipping a switch connected to the DAQ unit that told it to start saving data. Once riding conditions were met, the switch was flipped and relevant data was recorded. Short intervals of no loading were inserted between trials in order to differentiate the runs within a single test. Each loading condition was tested multiple times.

Results:

The principal stresses along the top of the chainstay as well as on the top of the main tube were calculated from the strain data for the various test cases. The axial stress along the top of the down tube was also found. Data taken from the side of the right chainstay (rosette gauge 2) was suspect and will be assessed in the future. Figures 4 through 6 are error bar plots of the three gauges that were analyzed for the different loading conditions. The plots reflect the mean of the stress with bars plus or minus one standard deviation from the mean. For the static and steady riding conditions, the overall mean and standard deviation is reflected. For the numeric results seen below it is reported as the average with the corresponding standard deviation in parentheses next to it. The hard acceleration cases display the mean of the peaks from each test run and the standard deviation between the different peak values. Also, for the numeric results the average peak value is followed by the standard deviation between the different peak values in parentheses. Note that compressive stresses are negative (-) and tension is positive (+). The state of stress within the frame was also modeled using FEA, and comparable results were calculated for the static and hard acceleration cases. A marker can be seen on some plots indicating the relative position of the FEA result to those found experimentally. The naming convention for the plots can be seen in Table 1. Numerical comparisons can be seen in Tables 2 through 4. It is important to note that because the second principal stress is a small value, the percent difference is usually quite large between the experimental and FEA results. So, the large percentage does not necessarily reflect the closeness of the results. A plot of stress versus time for the hard acceleration on level ground can also be seen in Figure 7.

Figure 4 shows the results for rosette gauge 1. The location of each gauge can be seen in Figure 33. The main principal stress for static, steady riding on smooth, medium, and rough surfaces, and hard acceleration riding level and uphill are as follows: -8.0(0.2), -9.0(.6), -9.2(.9), -5.0(1.9), -9.1(1.7), and -9.9(2.2) ksi. The secondary principal stress for these loading conditions are -0.6(.0), -0.8(.3), 0.2(1.5), 2.2(.2), 1.5(.2), and 1.4(.3) ksi, respectively. The FEA model predicted principal stresses of -7.4 and 0.0 ksi for the static situation and -8.3 and 0.2 ksi for the hard acceleration loads.

5 shows the results for rosette gauge 3. The main principal stresses for the loading conditions previously mentioned are as follows: -6.4(.1), -5.4(.4), -5.6(.6), -4.0(1.2), -4.6(.7), and -5.6(.8) ksi. The second principal stresses for these conditions are the following: -0.2(.0), -0.4(.2), -0.1(.0),-0.2(.2), 0.9(.3), and -1.1(.3) ksi. The FEA model predicted stresses of -6.2 and 0.4 ksi for the static situation and -7.8 and 0.1 ksi for the hard acceleration loads at this position.

6 shows the results for linear gauge 4. The average compressive stresses are -4.5(.0), -3.5(.3), -4.0(.4), -2.3(1.0), -4.6(.8), and -5.1(.8) ksi. The FEA model predicted stresses of -2.0 ksi for the static situation and -4.1 ksi for the hard acceleration loads at this position.

Table 1: Plot Naming Convention

Plot Key	
Abbreviation	**Meaning**
ssv	Average Value
pv	Peak Value
SL	Static Load
SR_SP	Steady Riding – Smooth Pavement
SR_MP	Steady Riding – Medium Pavement
SR_RP	Steady Riding – Rough Pavement
HA_LG	Hard Acceleration – Level Ground
HA_UH	Hard Acceleration – Uphill
SIG #1	Secondary Principal Stress for Rosette Gauge #
SIG #2	Primary Principal Stress for Rosette Gauge #
SIG #x	Axial Stress for Linear Gauge #

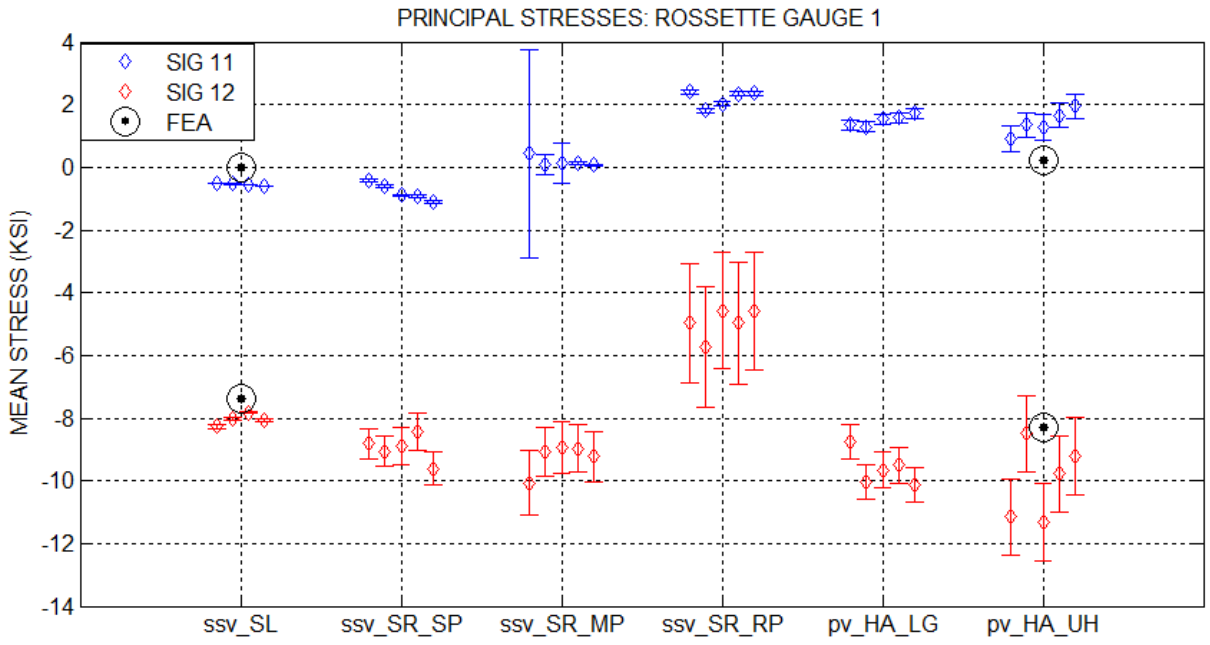

Figure 4: Top Right Chainstay – Principal Stresses with One Standard Deviation Error Bar

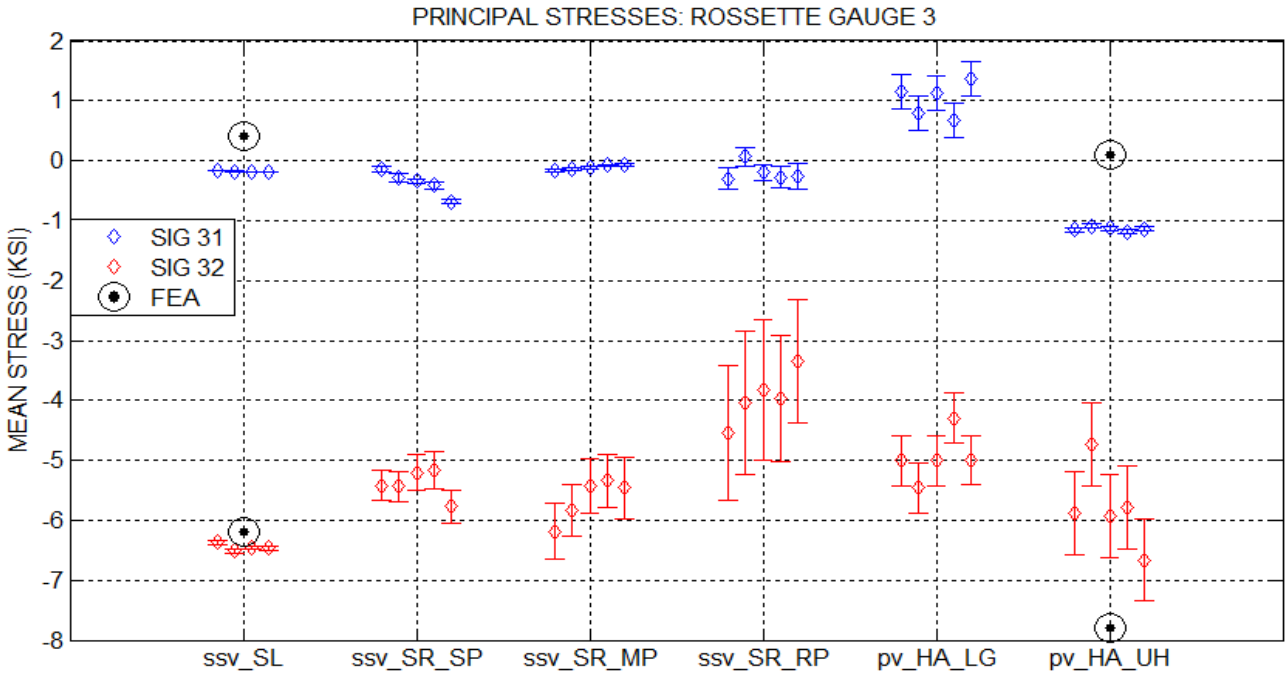

Figure 5: Main Tube Center – Principal Stresses with One Standard Deviation Error Bar

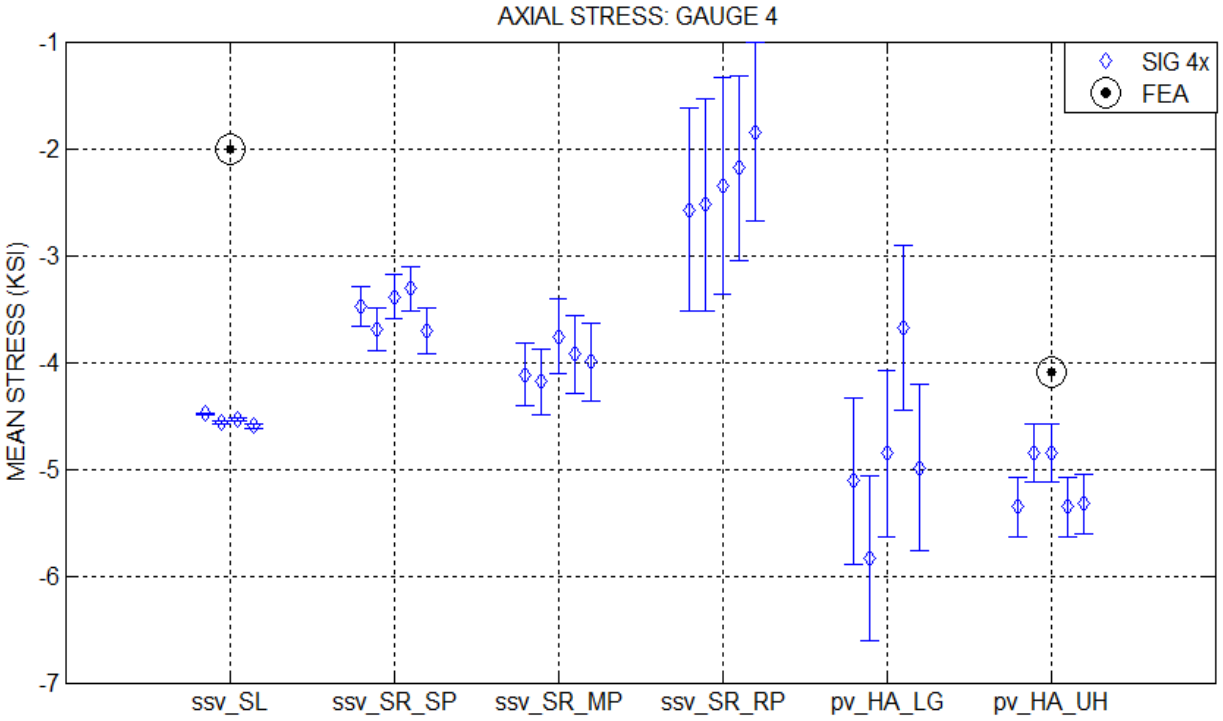

Figure 6: Down Tube – Axial Stress with One Standard Deviation Error Bar

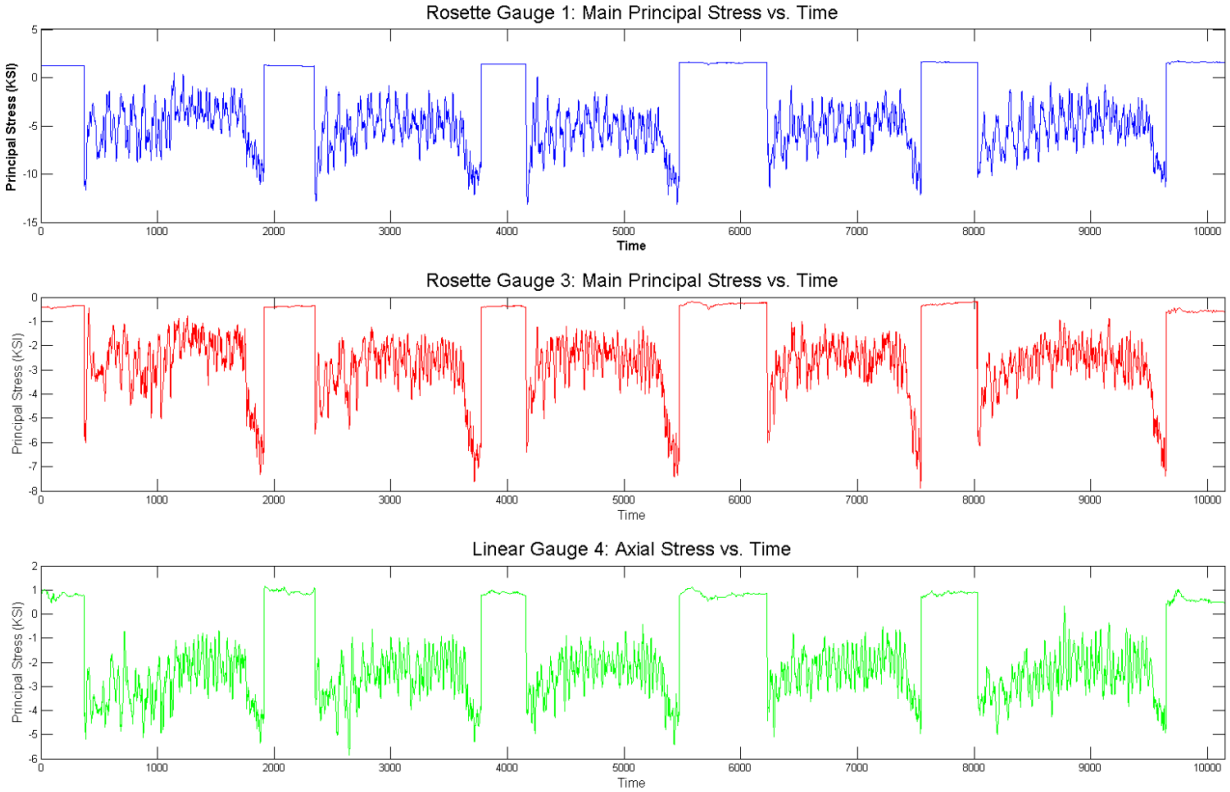

Figure 7: Main Stresses vs. Time

Table 2: Stresses for Different Loading Conditions

Stresses for Different Loading Conditions						
		Steady Riding – Surface			Hard Acceleration	
	Static (ksi)	Smooth (ksi)	Mid-Grade (ksi)	Rough (ksi)	Level (ksi)	Uphill (ksi)
Sig11	-0.6	-0.8	-0.2	2.2	1.5	1.4
Sig12	-8.0	-9.0	-9.2	-5.0	-9.1	-9.9
Sig31	-0.2	-0.4	-0.1	-0.2	0.9	-1.1
Sig32	-6.4	-5.4	-5.6	-4.0	-4.6	-5.6
Sig4x	-4.5	-3.5	-4.0	-2.3	-4.6	-5.1

Table 3: Principal Angles for Rosette Gauges – Note: Gauge 3 has +/- due to cyclic change

Principal Angles for Rosette Gauges - Degrees						
		Steady Riding – Surface			Hard Acceleration	
	Static	Smooth	Mid-Grade	Rough	Level	Uphill
Gauge 1	**36 (.2)**	**35 (.8)**	**36 (.8)**	**36 (1.4)**	**35 (2.4)**	**33 (4.9)**
Gauge 3	**37 (9.2)**	**+38 (9.6) -37 (9.0)**	**+39 (7.2) -41 (4.1)**	**+34 (10.9) -32 (9.0)**	**+25 (13.6) -27 (11.6)**	**+26 (9.8) -23 (12.8)**

Table 4: FEA Comparison

FEA Comparison						
	SL (ksi)	FEA 1G (ksi)	% Difference	HA_LG (ksi)	FEA HA-LP 3G (ksi)	% Difference
Sig11	-0.6	0.0	**107.6%**	1.5	0.2	**86.7%**
Sig12	-8.0	-7.4	**7.5%**	-9.2	-8.3	**9.8%**
Sig31	-0.2	0.4	**314.1%**	0.9	0.1	**88.9%**
Sig32	-6.4	-6.2	**3.3%**	-4.7	-7.8	**-66.0%**
Sig4x	-4.5	-2.0	**55.6%**	-4.7	-4.1	**12.8%**

Discussion:

Several interesting observations can be made based on the results of the experiment. More analysis was focused on the main principal stresses as they were the more relevant results. As previously mentioned, the second principal stress was often quite small, which often caused significant deviations in the results. Rosette gauge 1 was located on the right chainstay, at a position behind the seat mount. For this gauge, the maximum compressive stress increased from the static loading condition to the steady riding on smooth and midgrade pavement. There was a sizeable decrease (38% relative to static), however, in this principal stress when riding on rough pavement as seen in Table . This was most likely the result of the redistribution of the rider's weight due to increased pedaling force. The force the rider exerted on the back support of the seat increased as more force was applied to the pedals (more effort was required in order to maintain a constant speed on the rough surface). The back support of the seat is mounted is such a way that the load is applied at a position further back on the frame which can be seen in Figure 8. The point at which the members attached to the back of the seat connect to the frame is behind the strain gauge. The weight of the rider causes the frame to bend concave up, so as the load is distributed to a point further back on the frame, it decreased the concavity. For the hard acceleration cases, there was considerably more scatter in the data. The peak values obtained were very similar to the average values found for steady riding on smooth and midgrade pavement, with the difference between the two types of cases being less than 10%. This was also most likely a result of the rider's weight being distributed to different parts of the frame, such that the amount of compressive force experienced at the gauge location decreased.

Figure 8: Rear Seat Mount Support

For rosette gauge 3 on the main tube, the results were slightly different. It is important to remember, when considering these results, that the gauge was located on the main tube at a position in front of the main seat mount. As seen in Table , the maximum compressive stress for this gauge decreased from static loading to the steady riding on smooth, midgrade, and rough surfaces by 16%, 13%, and 38%, respectively. The cause of this decrease is most likely a result of the increased pedaling force. As opposed to the previous gauge, there was actually a decrease in all three load cases compared to the static situation. At a position between the seat and the pedals, that portion of the frame would bend concave up due to the weight of the rider. Once again, as the rider exerts force on the pedals, the redistribution of the weight tends to decrease the level of concavity, and subsequently the amount of stress registered at that gauge location. The difference in trend between the two gauges was most likely due to the frame segment being considered. Gauge 3 was between the seat and the pedals, rather than just behind the seat. For the hard acceleration cases the results were fairly similar to the steady riding values. As seen in in 2, on level ground and going uphill the peak of the main principal stress was less than the average static load value by 28% and 13%, respectively. A significant factor that had to be taken into account for this gauge was its proximity to the pedals. The axis along which the principal

stresses acted was prone to a sign change at regular intervals as seen in Table 3. This was simply due to which foot was applying force to the pedals, which would cause the shear force to change back and forth across the frame. Analysis of the principal angle using Equation 3 seems to indicate that the angle maintained a fairly consistent magnitude; however, it would abruptly change signs as expected.

The linear gauge on the down tube (gauge 4) showed a similar trend in values to those obtained for the main principal stress from rosette gauge 3. Gauge 4 only calculated the axial stress, but the magnitude of the stress followed a similar pattern for the different loading conditions. The axial stress, as seen in Table , decreased from static loading to steady riding on smooth, midgrade, and rough pavement by 22%, 11%, and 49%, respectively. The explanation for this decrease is more complicated than for the previous gauges. This particular gauge is on the down tube which connects the front fork to the main tube. It is just slightly in front of the pedals, so the effect previously described with increased force in that region shouldn't be the only factor. Something that adds complexity to the situation is the stiffness of the front fork and how it responds to variations in the road surface. Currently, the research has not reached a conclusion as to the cause for this decrease in stress. For the hard acceleration the results were more as expected as they increased compared to static by 2% and 13% for the level and uphill conditions, respectively.

The main purpose of this experiment was to verify the Finite Element Analysis model of the frame. The FEA software used was *CREO Pro/Mechanica*, by PTC. Several models were implemented. The first model used beam idealizations with point loads and constraints. The second model used shell idealizations and surface loads and constraints. Both models involved simplification of all loads, including the loading from the seat and pedal loads. Pedal loads were applied at the crank bearing locations. The magnitude and direction of these loads were calculated based on pedal force, chain ring size, crank arm angular orientation, and foot position. The assumed worst-case pedal load force and crank position was based on rider body orientation. The seat loads are complex and somewhat variable for actual riding. They depend on the rider size, weight, and body proportions as well as seat design. Assumptions regarding distributions were made to simplify the analysis. First, the system was modeled with just the weight of the rider included acting in a 1G system with no motion. This model should line up closely with the results found experimentally for the static loading condition. The other scenario modeled was a 3G load including the torque the rider exerted on the pedals. This model should approximate the hard acceleration cases; however, the complexity of those loading situations and the deviations in the results made extremely close comparison quite unlikely. The results of the FEA analysis can be seen in Table 4.

For the static loading condition the experimental and FEA results compared as follows: For rosette gauge 1, the difference between experimental and FEA values for the main principal stress was 7.5%, with the actual difference being approximately 0.6 ksi. The second principal stress had the same actual difference, but the percent difference was considerably greater because the average values were extremely small, and thus any variation produced large deviations. For the rosette gauge 3, the difference was 3.3% for the main principal stress. As before the second principal stress showed a very large percent difference, but the actual variation in the values was

only 0.6 ksi. For linear gauge 4, the difference was 55.6%, which was quite large. At this point in the research, the answer for this discrepancy is still undetermined.

For the hard acceleration case on level ground the experimental and FEA results compared as follows: For rosette gauge 1, the difference between the main principal stress and FEA values was 9.8%, with the actual difference being approximately 0.9 ksi. As in the previous loading condition, there were considerable percent differences between the second principal stresses, but this was simply a result of the values being quite small, and thus any variation produced a large deviation. The actual difference was only 1.3 ksi. Originally, the results for the model were considerably different from the experimental data; however, upon testing to determine the force actually being applied to the pedals, we discovered that we had significantly overestimated that load simplification within the FEA model. After critiquing the model, the results obtained were much more favorable. For rosette gauge 3, the difference was 66.6% for the main principal stress and 88.9% for the second. These variations were larger than hoped for, but given the complexity of the loading situation and the proximity of the gauge to the pedals, it was not altogether unexpected. For linear gauge 4, the difference was 12.8%. When we originally tested this loading condition in the FEA model, there was a much larger difference. We discovered that in order to accurately predict the situation, the front fork stiffness had to be included in the model. As mentioned before the results for the static loading condition were considerably different from the experimental data, so more work continues in this area as we learn what factors affect the stress in different parts of the frame.

Conclusion:

The states of stress of a bicycle frame were successfully found experimentally, being confirmed by multiple runs under each loading condition. Variations in the road surface, pedaling force applied by the rider, and the weight of the rider all affected the state of stress within the frame. As expected there was significantly more scatter in the data taken on a rough surface and when pedaling at max acceleration. The values found using FEA were comparable to those found experimentally. Based on the agreement between the two methods, the use of FEA load cases to predict stresses in pedal cycle frames was verified.

Bibliography:

[1] Holman, J.P., 2001, *Experimental Methods for Engineers*, 7th ed., McGraw Hill, New York, NY, Chap. 10.